Ceramics International 48 (2022) 1326–1339

Contents lists available at ScienceDirect

Ceramics International

journal homepage: www.elsevier.com/locate/ceramint

Rapid synthesis of eggshell derived hydroxyapatite with nanoscale characteristics for biomedical applications

D. Muthu [a], G. Suresh Kumar [b], M. Gowri [a], M. Prasath [c], V. Viswabaskaran [d], V.S. Kattimani [e], E. K. Girija [a,*]

[a] Department of Physics, Periyar University, Salem, 636 011, Tamil Nadu, India
[b] Department of Physics, K.S. Rangasamy College of Arts and Science (Autonomous), Tiruchengode, 637 215, Tamil Nadu, India
[c] Department of Biotechnology, Bharathiar University, Coimbatore, 641 046, Tamil Nadu, India
[d] VB Ceramic Consultants, Chennai, 600 041, Tamil Nadu, India
[e] Department of Oral and Maxillofacial Surgery, Sibar Institute of Dental Sciences, Guntur, 522 509, Andhra Pradesh, India

ARTICLE INFO

Keywords:
Microwave reactor
Eggshell
Organic modifiers
Mesoporous
Carbonated hydroxyapatite

ABSTRACT

Utilizing eggshells to synthesize a value added product like nanocrystalline hydroxyapatite (HA) has received a lot of attention from researchers since they are composed of $CaCO_3$ with biologically essential trace elements such as Mg, Si, *etc*. Different biomedical applications need HA with appropriate nanoscale characteristics like crystallinity, particle size, morphology, surface area, mesoporous nature, *etc*. The same can be achieved by tuning the reaction parameters, choosing a suitable mode of preparation and utilizing organic modifiers. Here, we report the rapid synthesis of eggshell derived HA in the presence different organic modifiers using a custom built microwave reactor employing the previously optimized parameters. The synthesis process is relatively rapid and gets completed in 5 min. The absence of an organic modifier yielded inhomogeneous size nanorods in the range of 40 – 600 nm. Ethylenediaminetetraacetic acid (EDTA) assisted synthesis resulted in a flower like 1.67 ± 0.12 μm sized HA. Whereas polyethylene glycol 6000 (PEG) and cetyltrimethylammonium bromide (CTAB) assisted synthesis produced aggregated nanorods of length 31 ± 8 and 68 ± 20 nm, respectively. While the synthesis with trisodium citrate dihydrate (TSC) resulted in needles of HA with typical length of 32 ± 8 nm. Presence of Na, Mg and Si trace elements are confirmed from the composition analysis. All the samples are found to be mesoporous in nature. The *in vitro* cell culture experiment carried out using fibroblast NIH 3T3 cell line clearly revealed equal or higher cell viability for the samples synthesized in presence of organic modifiers as compared to sample produced without organic modifier. Thus, from the present study we find that the synthesis of eggshell derived HA using different organic modifiers *via* a custom built microwave reactor can be a potential approach for the rapid preparation of precursor materials with suitable nanoscale characteristics for developing bone fillers, drug/protein delivery carriers, tissue engineering scaffolds, *etc*.

1. Introduction

Hydroxyapatite [HA, $Ca_{10}(PO_4)_6(OH)_2$] is the dominant mineral phase in the human skeletal system [1,2]. Synthetic HA has been widely used in bone tissue engineering and other biomedical applications in dentistry and orthopaedics owing to its compositional and structural similarity with the mineral phase of bone and teeth [3,4], consequently its excellent bioactive and cytocompatible nature [5]. In addition, the usage of HA is not only limited to the biomedical field, but also used as an adsorbent for organic dyes and heavy metal ions, catalyst, electret and proton conductor [6–8]. Current scenario is the development of HA based materials with enhanced properties through nanotechnology by utilizing novel physical/chemical processes [6,9]. Nanoscale characteristics of HA should be optimized to achieve better performance for different biomedical applications [10]. Particularly, the physicochemical and biological properties of mesoporous HA nanostructure is different from bulk materials [9,11]. Moreover, factors such as crystallinity, particle size, morphology and surface area of mesoporous HA nanostructures play a vital role in biomedical applications [12]. Hence, significant efforts are being made to control the size and shape of HA

* Corresponding author.
E-mail address: girijaeaswaradas@gmail.com (E.K. Girija).

https://doi.org/10.1016/j.ceramint.2021.09.217
Received 7 July 2021; Received in revised form 16 September 2021; Accepted 21 September 2021
Available online 23 September 2021

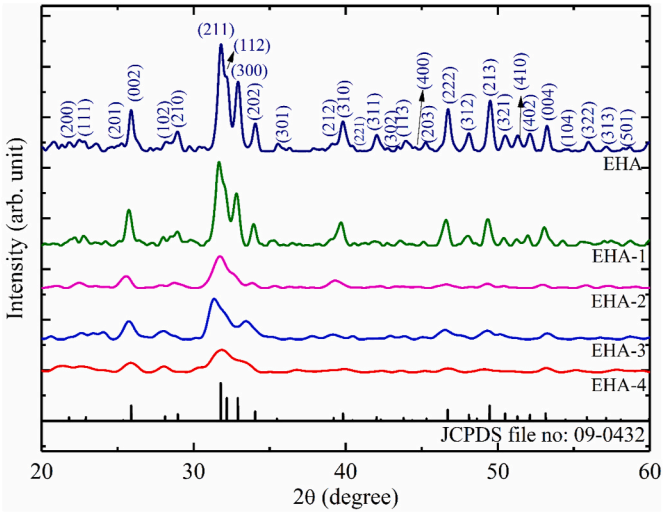

Fig. 1. XRD patterns of the samples prepared without organic modifier (EHA), with organic modifiers (EHA-1, EHA-2, EHA-3 and EHA-4) and simulated data for HA (standard JCPDS no: 09–0432)

Table 1
Lattice parameters, crystallite size, crystallinity and *c/a* values of prepared samples.

Sample code	Lattice parameters (Å)		Average crystallite size (nm)	Average crystallinity (X_c)	*c/a* ratio
	a=b=9.4180	c=6.8840			
EHA	9.4160	6.8769	54 ± 3	3.61 ± 0.6	0.7304
EHA-1	9.4389	6.9147	42 ± 2	1.73 ± 0.5	0.7325
EHA-2	9.3961	6.9748	23 ± 5	0.29 ± 0.1	0.7423
EHA-3	9.4301	6.9137	28 ± 2	0.31 ± 0.1	0.7331
EHA-4	9.4074	6.8865	21 ± 3	0.20 ± 0.1	0.7320

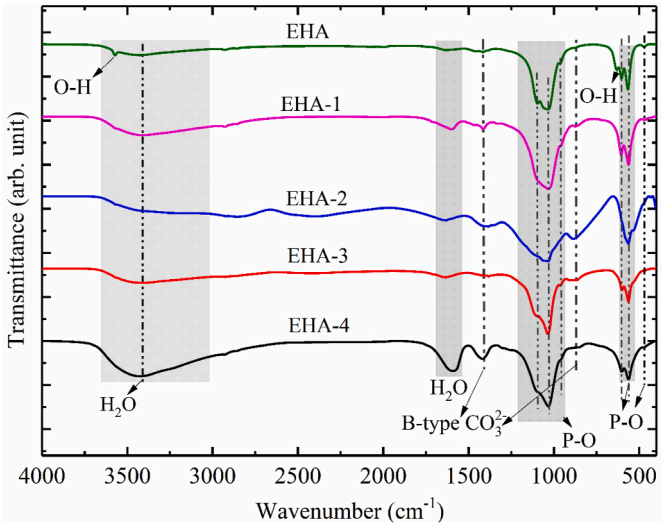

Fig. 2. FTIR spectra of samples prepared without the organic modifier (EHA) and with organic modifiers (EHA-1, EHA-2, EHA-3 and EHA-4)

nanoparticles.

It was found that the preparation method dramatically influences the characteristics of the HA produced. The reaction parameters such as temperature, pH, ageing time, *etc.* are also important to synthesize HA with superior nanoscale characteristics [13]. Moreover, different organic modifiers and surfactants were also effectively used to control the characteristics of nano HA since calcium and phosphate ions can easily interact with organic species during the synthesis [14]. Several methods such as chemical precipitation [15], sol-gel [16], microemulsion [17], hydrothermal [11], electrochemical [18], microwave [19] and solid state method [20] were reported for the synthesis of nano HA. Among the different synthesis methods, the microwave technique is an efficient and straightforward method to prepare HA nanoparticles rapidly. In the past few decades, many research papers haves been published on the synthesis of HA using the conventional domestic microwave oven [19].

Several researchers have utilized various biogenic sources such as corals, eggshells, fish scales, seashells, animal bones, *etc.*, as a calcium source to synthesize nanocrystalline HA [15]. Among them, eggshells are a highly preferred calcium source since they are mainly composed of 94% calcium carbonate ($CaCO_3$) with trace elements such as magnesium (Mg), silica (Si), *etc.,* [21]. Annually worldwide large quantities of eggshells are discarded as landfills from restaurants, hatcheries, *etc.,* [22]. Moreover, when compared to HA derived from commercial reagents, eggshell derived HA exhibited superior bioactivity, excellent osteoconductivity, osteoinductivity and cell proliferation and is often attributed to the presence of trace elements that originated from the eggshell source [23]. Egg white and eggshell based hydrogel composite scaffold fabricated by Huang et al. exhibited better bioactivity [24]. Bone cement and 3D scaffold prepared from eggshell derived calcium phosphates were reported to be suitable for hard tissue regeneration, as it has a good cement setting behaviour, compressive strength, biocompatibility and better osteogenic differentiation as compared to synthetic bone cement/scaffold [25,26]. Also, eggshell derived nano HA reinforced with the polymer to fabricate composite membrane or scaffolds revealed enhanced thermal, mechanical and biological properties compared to pure polymer membrane/scaffold [27–29]. Protein delivery, drug delivery and waste water remediation have also been studied using eggshell derived HA [7,30,31].

Although several reports are available on the synthesis of nano HA from eggshell through different techniques, microwave assisted chemical precipitation is highly preferred by several researchers due to its advantages like simplicity, economical, rapid process, reproducibility, high yield, *etc.,* [19]. Also, recent research suggested that microwave technique directly results in mesoporous HA nanostructures even without employing hard templates or surfactants [32,33]. Nanoscale HA with mesoporous characteristics have received significant attention in developing drug/protein carriers, implants and tissue engineering scaffolds. Even though mesoporous HA can be obtained *via* microwave technique, we can control the size, morphology and mesoporous characteristics of HA using different organic reactive molecules. Recently, we reported the impact of various reaction parameters for HA synthesis from eggshell waste using lab scale and a custom built pilot scale microwave reactor made using four magnetrons (1.1 kW per magnetron) [34]. The custom built pilot scale microwave reactor significantly reduced the microwave irradiation time as compared to the domestic microwave oven used as a lab scale reactor. The objective of the present work is to study the formation of eggshell derived HA using the above mentioned custom built pilot scale microwave reactor in the presence of reactive organic compounds such as EDTA, PEG, TSC and CTAB employing the necessary parameters optimized in the previous work.

2. Experimental

All the chemicals, namely nitric acid (HNO_3), disodium hydrogen phosphate (Na_2HPO_4), sodium hydroxide (NaOH), ethylenediaminetetraacetic acid ($C_{10}H_{16}N_2O_8$), polyethylene glycol 6000 ($H(OCH_2CH_2)nOH$), trisodium citrate dihydrate ($C_6H_9Na_3O_9$) and cetyltrimethylammonium bromide ($C_{19}H_{42}BrN$) were analytical reagent grade acquired from Merck, India. All reagents were used without further purification and double distilled water was employed as the solvent. Broiler eggshells were utilized as the calcium source in the present study due to its abundant availability in India.

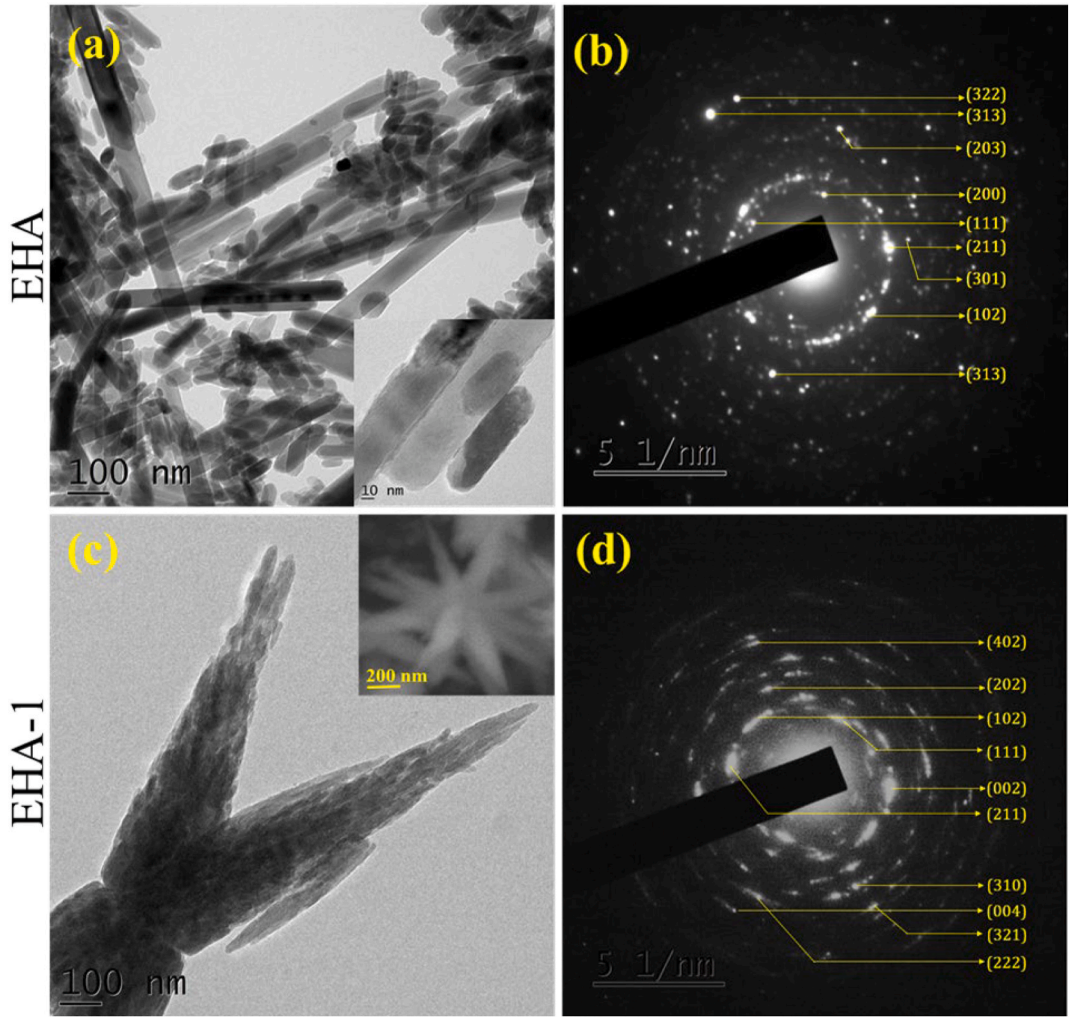

Fig. 3. HRTEM images and SAED pattern of EHA and EHA-1. Inset in Fig. 3(c) is the SEM image of EHA-1.

2.1. Custom built pilot scale microwave reactor

The pilot scale microwave reactor used in this study was developed by modifying conventional microwave furnace (supplied by VB ceramic consultants, Chennai, India). The reaction vessel used for the reactor replaced the susceptor of the microwave furnace. The reactions were conducted in water as the dielectric medium. The reaction vessel was designed in such a way with the lid having the provisions for inlet and outlets. A suction pump is connected to the reaction vessel for releasing the pressure. There are four magnetrons (1.1 kW/magnetron, 2.45 GHz) of which two operate at a time, one on both side to allow homogeneous radiation inside the reactor. Hence, microwave power during the operation is 2.2 kW. After completing the reaction, the instrument is manually switched off as the sensing unit of microwave furnace that allows automatic power cut-off cannot be used when the instrument is operating in reactor mode.

Eggshells were collected, cleaned manually and then placed in a furnace at 900 °C for 1 h. At this temperature, eggshells transform into calcium oxide (CaO) by evolving carbon dioxide (CO_2) according to the following equation (1).

$$CaCO_3 \xrightarrow{\Delta} CaO + CO_2\uparrow \quad (1)$$

The eggshell derived CaO (0.1 M) was dissolved in nitric acid (0.2 M) to form calcium nitrate solution (eqn. (2))

$$CaO + 2\,HNO_3 \rightarrow Ca(NO_3)_2 + H_2O \quad (2)$$

0.06 M disodium hydrogen phosphate solution was prepared by dissolving an appropriate amount of Na_2HPO_4 in double distilled water. Obtained calcium nitrate solution was stirred vigorously at room temperature to which Na_2HPO_4 solution was added dropwise while maintaining the pH of the reaction mixture above 10 using NaOH and was stirred for 30 min at room temperature. The expected chemical reaction is given in equation (3),

$$10Ca(NO_3)_2 + 6Na_2HPO_4 + 8NaOH \rightarrow Ca_{10}(PO_4)_6(OH)_2 + 20NaNO_3 + 6H_2O \quad (3)$$

The obtained reaction mixture (100 ml) was transferred into the microwave reactor chamber followed by microwave irradiation at 2.2 kW for 5 min. The resulting white precipitate acquired was centrifuged (6000 rpm) and washed 6 times with double distilled water to remove the by-products, followed by drying at 110 °C for 5 h in a hot air oven. Finally, dried cakes were crushed using mortar and pestle to get white powder which is named as EHA. Experiments were also carried out in presence of EDTA (0.2 M) [34], PEG (1 wt.%) [35], TSC (0.0333 M) [36] and CTAB (0.06 M) [37] in which the former three organic modifiers were added along with the calcium reagent while the latter one was mixed with phosphate reagent. The individual organic modifier concentration mentioned above was chosen based on the optimized concentration available in the literature. The samples prepared using EDTA, PEG, TSC and CTAB were named EHA-1, EHA-2, EHA-3 and EHA-4 respectively.

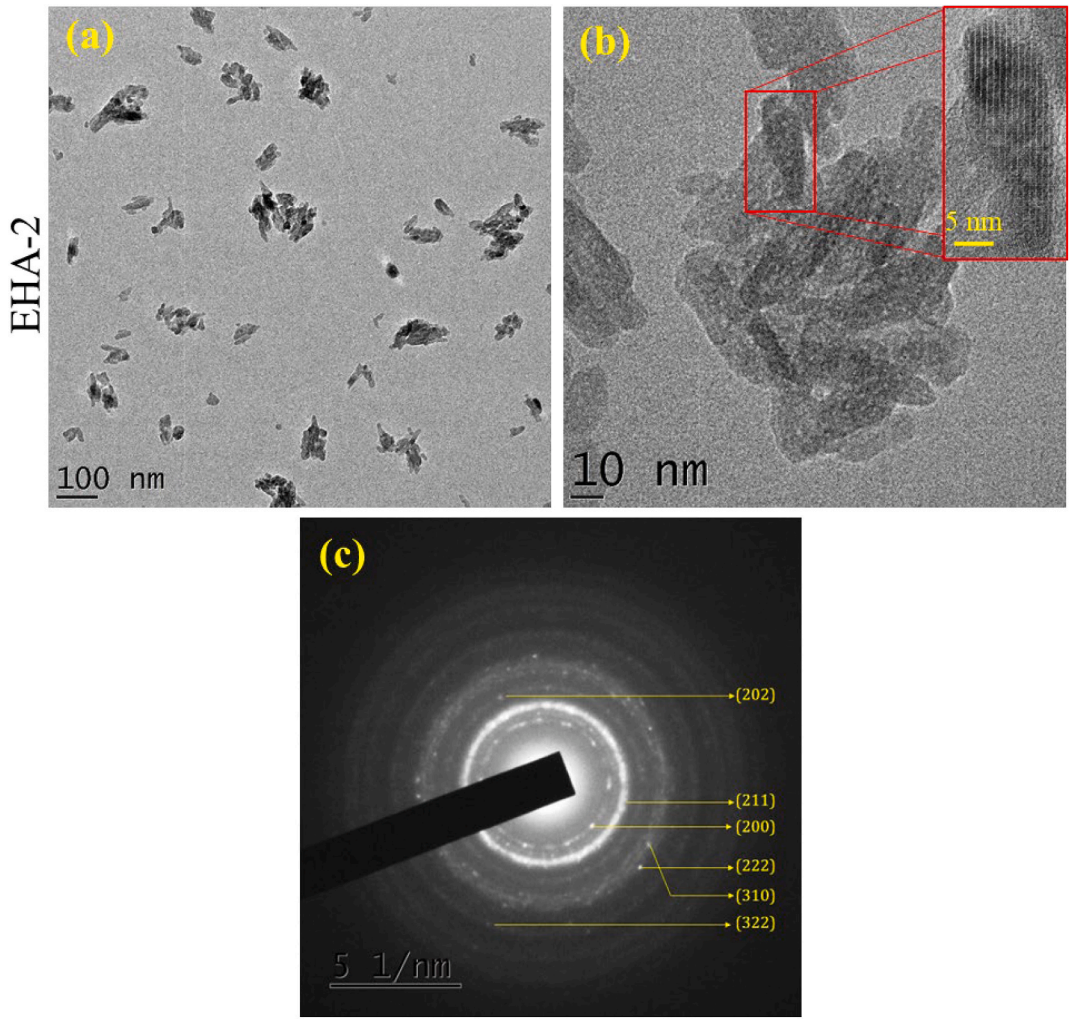

Fig. 4. (a, b) HRTEM images (c) SAED pattern of EHA-2 sample

2.2. Characterization

Phase purity, crystalline nature and lattice parameters of the synthesized samples were analysed by powder X-ray diffraction (XRD) technique (Rigaku MiniFlex-II) using monochromatic Cu-kα radiation (1.5406 Å). The powder XRD patterns were recorded in the range between $20^\circ \leq 2\theta \leq 60^\circ$ with a scan speed of 10°/minute and step size of 0.02°. In addition, the full width at half maximum (FWHM) was calculated from the XRD pattern to measure the average crystallite size by the Scherrer method [38].

The functional groups present in the prepared samples were examined using Fourier transform infrared spectroscopy (FTIR). Powder samples were ground with KBr and pressed into a disc using a pelletizer. The FTIR spectra were recorded from 4000 to 400 cm^{-1} using a Perkin Elmer RX1. Particle size, morphology and crystalline nature of the prepared samples were analysed using high resolution transmission electron microscopy (HRTEM- JEOL/JEM 2100) and selected area electron diffraction (SAED). For HRTEM analysis, small amount of sample was dispersed in ethanol under sonication for 30 min and 1 μl of the dispersed sample was placed on the carbon coated copper grid. The elemental composition of the samples was analysed using energy dispersive X-ray analyser (EDAX) by INCA, Oxford instruments. Scanning electron microscopy (SEM, Carl Zeiss - EVO 18) was used to analyse the surface morphology of the prepared samples.

The pore size, pore volume and surface area of the samples were determined using the N_2 adsorption-desorption isotherm method (Micromeritics ASAP 2020). In addition, thermogravimetric analysis (TGA) and differential scanning calorimetry (DSC) of synthesized products was carried out from 34 to 1200 °C with heating rate of 10 °C/minute using Jupiter (NETZSCH STA F3) instrument.

2.3. Cytocompatibility assay

The cytocompatibility of samples was tested with fibroblast NIH 3T3 cell lines (purchased from National Centre for Cell Science (NCCS), Pune, India) by MTT assay. The fibroblast NIH 3T3 cells were cultured with 10% of fetal bovine serum (FBS) and 1% of penicillin-streptomycin followed by incubation at 37 °C with the humidified atmosphere in 5% of CO_2. The cultured fibroblast cells were sowed at a density of 1×10^5 cells/ml in 96 well tissue culture plate and incubated at standard culture settings (37 °C, 5% of CO_2 and 95% air) for 24 h. After incubation, synthesized powder samples were added into tissue culture plate at various concentrations such as 50, 100, 250 and 500 μg/ml and then incubated at 37 °C for 24 h in CO_2 incubator. Thereafter, 15 μl of MTT and phosphate buffered saline (PBS) was added to 96 well plate and then incubated at 37 °C for 4 h in a CO_2 incubator. After this, the supernatant of MTT solutions was discarded and the obtained formazan crystals were dissolved in 100 μl of dimethyl sulfoxide (DMSO) and the optical density (OD) was measured at 570 nm using a microplate reader. The percentage of viable cells was calculated from the following equation (4)

$$Percentage\ of\ cell\ viability = \left(\frac{OD_{sample}}{OD_{control}}\right) \times 100 \quad (4)$$

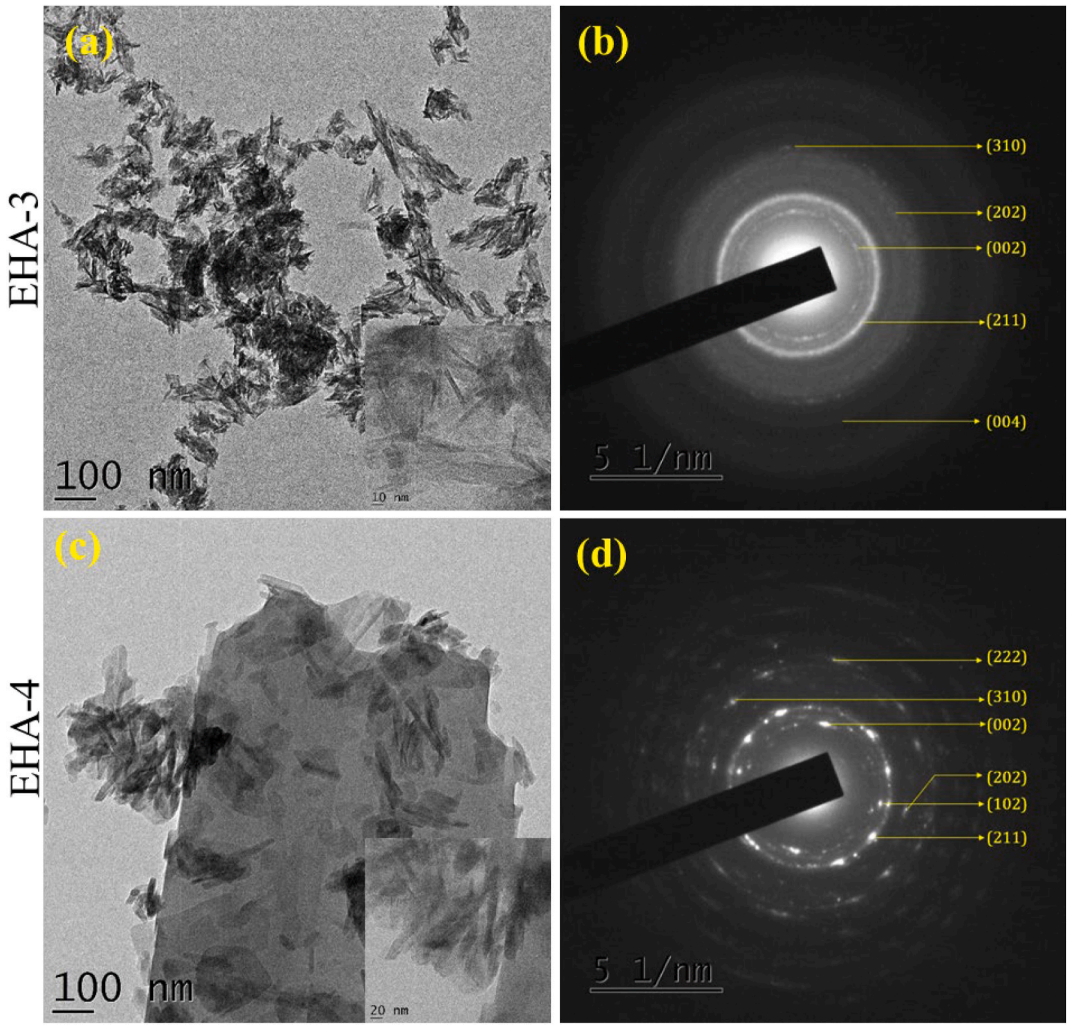

Fig. 5. HRTEM images (a & c) SAED pattern (b & d) of EHA-3 and EHA-4 sample

Table 2
Elemental composition of the prepared samples.

Sample code	Elements (at.%)					Ca/P
	Ca	P	Na	Mg	Si	
EHA	11.50	07.64	0.41	0.23	0.16	1.51
EHA-1	10.61	07.48	0.74	0.18	0.18	1.42
EHA-2	15.03	10.29	2.81	0.57	0.27	1.46
EHA-3	12.47	08.37	0.23	0.03	0.18	1.49
EHA-4	06.47	04.72	0.22	0.05	0.13	1.37

where, OD_{sample} is the optical density of cells with powder sample and $OD_{control}$ is the optical density of cells without sample.

2.4. In vitro cell attachment study

300 mg of prepared powder sample was made into a disc of about 13 mm diameter and 1 mm height using pelletizer by applying pressure at 20 MPa. The prepared disc samples were transferred to 6 well tissue culture plate. Fibroblast NIH 3T3 cells were cultured in 96 well plate at a density of 1×10^5 cells per well in Dulbecco's modified eagle medium (10% of FBS and 1% of penicillin-streptomycin) under incubation at 37 °C for 24 h in CO_2 incubator. 200 μl of the above cultured cells were seeded on the surface of the disc and incubated at 37 °C for 24 h in a CO_2 incubator. Then, the culture media was removed and the samples were washed with PBS and the discs were fixed with 4% of glutaraldehyde solution for 30 min followed by slow dehydration in ethanol of concentration 70%, 80%, 90% and 100% and dried at room temperature. Then, the dried samples were sputter coated with gold for 10 min to observe cell attachment on the surface using field emission scanning electron microscopy (FESEM, JEOL JSM-6390L).

3. Results and discussion

3.1. XRD

Fig. 1 shows the powder XRD patterns of samples prepared without and with the organic modifier. From the obtained XRD patterns we have seen that all five samples exhibited the characteristic diffraction peaks of HA (JCPDS file no: 09–0432 with hexagonal structure) without any other calcium phosphate phases. Pristine EHA (sample prepared without organic modifier) sample exhibit resolved peaks in between 30 and 35°. However, a significant decrease in the intensity of the diffraction peaks was observed for samples prepared with organic modifier EHA-1, EHA-2, EHA-3 and EHA-4. Moreover, the broadness of the diffraction peaks was found to increase for EHA-1, EHA-2, EHA-3 and EHA-4. These results clearly indicate that the presence of an organic modifier during the sample preparation plays a crucial role in modulating crystallization and control the growth of HA under microwave irradiation. The calculated average crystallite size and crystallinity of EHA, EHA-1, EHA-2, EHA-3 and EHA-4 are given in Table 1. It is interesting to note that PEG, TSC

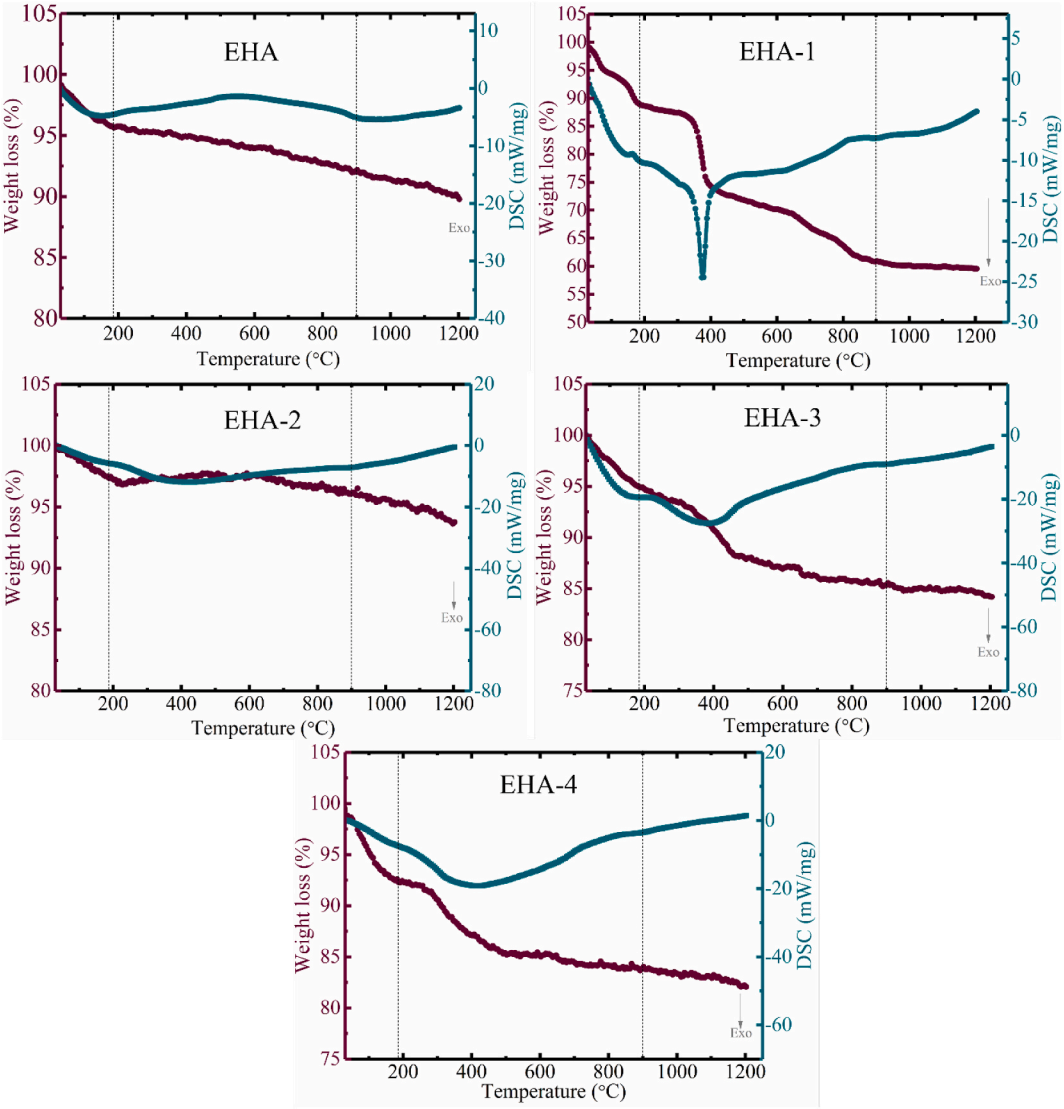

Fig. 6. TGA/DSC curves of the prepared samples

Table 3
Weight loss percentage of the prepared samples.

Sample code	Weight loss (%)			Total weight loss (%) (34–1200 °C)
	Step-I (34–180 °C)	Step-II (180–900 °C)	Step-III (900–1200 °C)	
EHA	4.26	3.58	2.38	10.22
EHA-1	11.03	28.07	1.36	40.46
EHA-2	2.51	1.33	2.41	6.25
EHA-3	5.04	9.42	1.36	15.82
EHA-4	7.43	8.56	1.93	17.92

and CTAB highly inhibited the crystallization of HA when compared with EDTA. Lattice parameters and lattice distortion of prepared samples were calculated and listed in Table 1. Significant difference in the crystallite size and crystallinity were found in between the prepared samples, which also confirm that organic modifiers can play a vital role in crystallization of HA by making interaction with calcium/phosphate precursor [13].

3.2. FTIR

FTIR spectra of samples prepared without and with organic modifiers are shown in Fig. 2. In the FTIR spectra the doublet peak observed at 604 and 566 cm^{-1} corresponds to the characteristic bending mode of phosphate (PO_4^{3-}) group of HA. Also, other phosphate peaks of symmetric and antisymmetric stretching vibrations appeared at 962 and 1030-1120 cm^{-1} respectively. The small peak detected for all the samples at 475 cm^{-1} is assigned to the bending mode of PO_4^{3-} group. The peaks that are present at 631 and 3572 cm^{-1} are ascribed to the characteristic OH^- group of HA and they are very sensitive to the crystallinity of HA [38]. Importantly, these peaks are not clearly visible in the FTIR spectrum of EHA-1, EHA-2, EHA-3 and EHA-4 due to their relatively poor crystalline nature which agrees with XRD results. Broad absorption band centred at 3420 cm^{-1} and a small band in between 1600 and 1645 cm^{-1} are ascribed to the stretching and flexural modes of adsorbed H_2O molecules and they are observed for all samples. The band at 1420 cm^{-1} and a small peak at 879 cm^{-1} are assigned to carbonate (CO_3^{2-}) group, which is acquired from the atmosphere during sample preparation (alkaline condition). The observed positions of carbonate peaks indicate that it is substituted for phosphate group in HA and formed as B-type carbonated HA [39].

3.3. HRTEM

Fig. 3(a) and (b) shows the HRTEM images and selected area electron

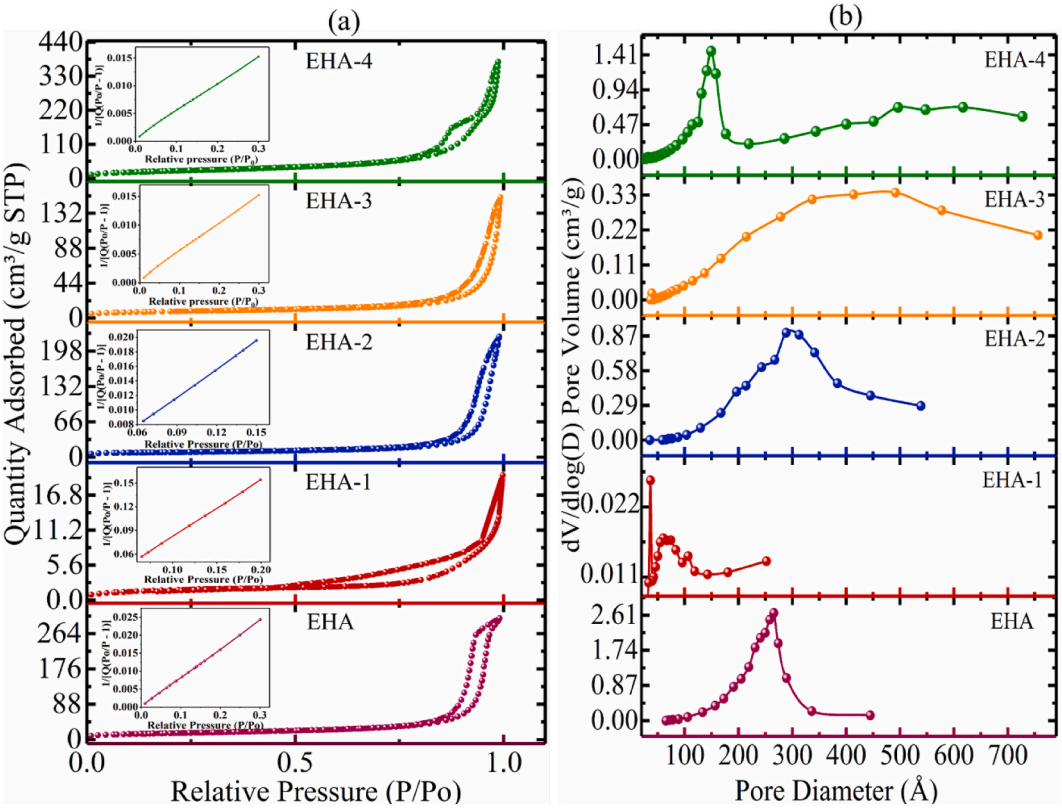

Fig. 7. (a) N_2 adsorption/desorption isotherm (inset BET surface area plot), (b) BJH pore size distribution of prepared samples

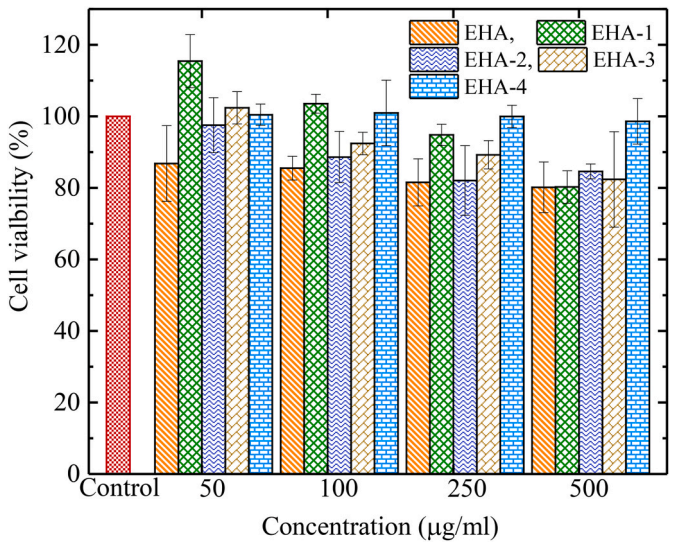

Fig. 8. Cell viability percentage of prepared samples with fibroblast NIH 3T3 cells

diffraction (SAED) pattern of EHA. HRTEM images of EHA clearly indicate that it consists of inhomogeneous rod like particles with clear boundaries. The average length and width of particles was calculated as 40 – 600 nm and 34 ± 10 nm respectively (Image J). SAED pattern of the EHA sample (Fig. 3(b)) reveals bright spots arranged in continuous ring which is owing to its polycrystalline nature and it is indexed with Miller's planes observed in XRD.

HRTEM, SEM images and SAED pattern of EHA-1 are shown in Fig. 3 (c) and (d). The SEM (inset in Fig. 3(c)) morphology of obtained EHA-1 sample shows the flower like structure with size of about 1.67 ± 0.12 μm. SEM observation of the sample synthesized using EDTA exhibited a flower like structure as reported in our previous work [34] which is shown in the inset of Fig. 3(c). A more close observation of an individual flake of the flower using HRTEM is shown in Fig. 3(c). Fig. 3(d) shows the SAED pattern of EHA-1 sample which is exhibiting continuous ring of diffused spots that represents the polycrystalline nature of EHA-1. Moreover it shows clear reflections from (402), (202), (102), (111), (002), (211), (310), (004), (321) and (222) Miller's planes of HA.

HRTEM pictures in Fig. 4(a) and (b) display the PEG assisted synthesized EHA sample (EHA-2). It exhibited rod shape with aggregates containing less number of nanoparticles of length and width 31 ± 8 nm and 8 ± 1 nm respectively. Remarkably, individual particles of EHA-2 sample contained pores of ~5 nm as can be seen from Fig. 4(b) (inset at top right corner). A magnified image of EHA-2 in Fig. 4(b) shows that the obtained nanoparticles are almost homogeneously sized. The SAED pattern of EHA-2 is made up of continuous rings with lucid spots revealing the formation of polycrystalline material.

From the HRTEM images of EHA-3 it is observed that the sample consists of highly agglomerated needle like nanoparticles having a length of about 32 ± 8 nm and width 3 ± 1 nm (Fig. 5(a)). EHA-3 exhibits polycrystalline nature which was confirmed from the lucid ring observed in the SAED pattern (Fig. 5(b)). HRTEM image (Fig. 5(c)) of EHA-4 exhibits highly aggregated nanorods of 68 ± 20 nm length and 10 ± 3 nm width. Fig. 5(d) shows the SAED pattern of EHA-4 containing bright spots arranged in ring pattern indicating the polycrystalline nature of the sample.

3.4. EDAX

The compositional analysis on the as synthesized powders was studied using EDAX. The prepared samples are composed of elements such as calcium (Ca), phosphorus (P), sodium (Na), magnesium (Mg), silicon (Si), carbon (C) and oxygen (O). The elemental composition of the synthesized samples examined by EDAX is given in Table 2. The Ca/

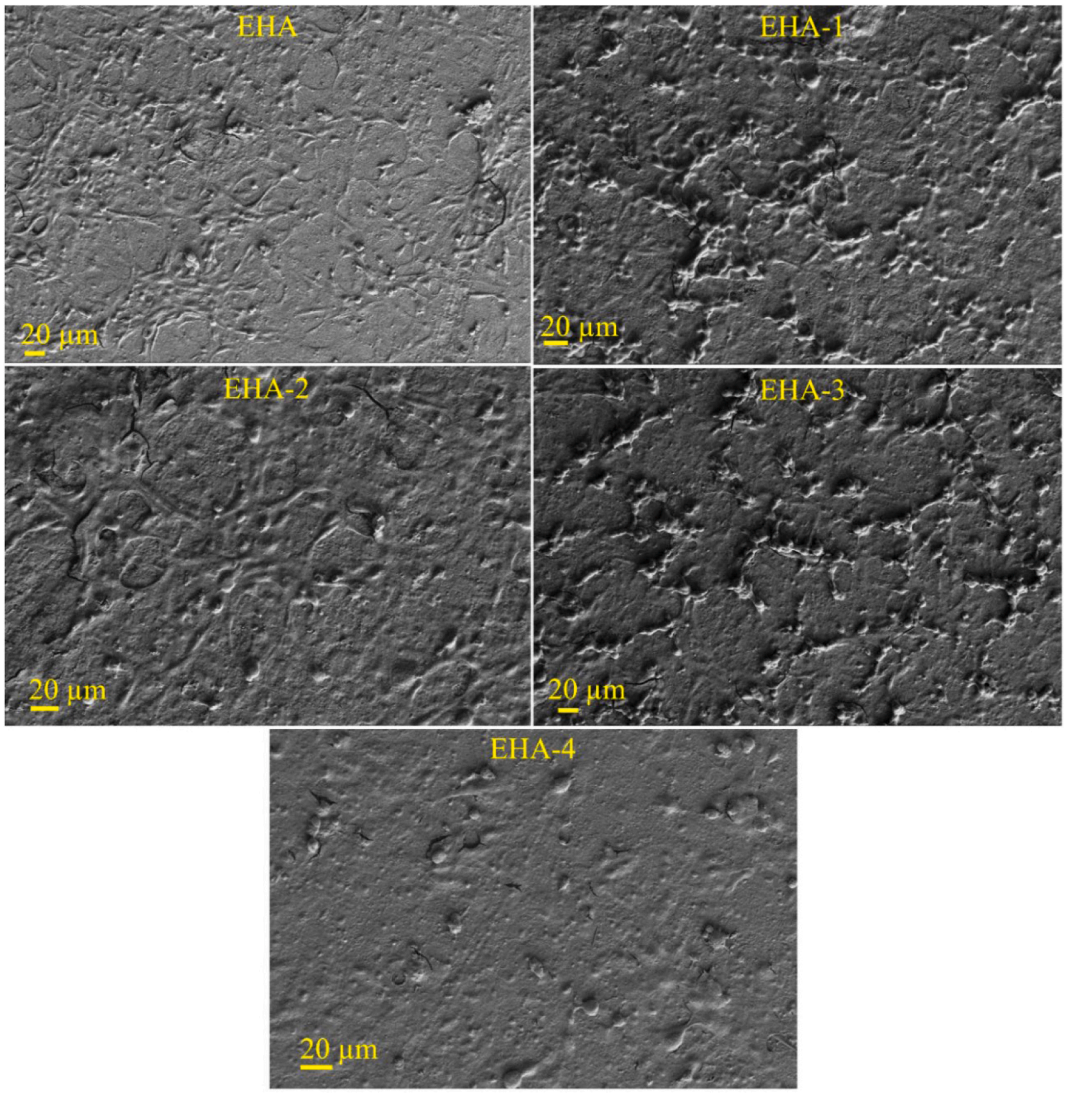

Fig. 9. FESEM micrographs of fibroblast NIH 3T3 cell adhered on the prepared samples disc surface.

P ratio obtained for the samples is 1.51, 1.42, 1.46, 1.49 and 1.37 respectively for EHA, EHA-1, EHA-2, EHA-3 and EHA-4. The obtained Ca/P ratio of the powder samples are less than 1.67 confirming that the synthesized samples are indeed non-stoichiometric HA.

Analysis of the elemental composition of chemically untreated eggshell was done by EDAX. The eggshell studied was found to be composed of elements such as calcium (13.8 at.%), phosphorus (0.3 at. %), sodium (0.9 at.%), magnesium (0.7 at.%), silicon (0.2 at.%), carbon (27.2 at.%), oxygen (55.9 at.%), fluorine (0.8 at.%) and iron (0.2 at.%). The eggshell was chemically processed to obtain HA, which contains trace elements such as magnesium, silicon and sodium. Trace elements in the prepared HA nanoparticles might be mostly contributed by the eggshell.

3.5. TG/DSC

TGA and DSC plots of the EHA, EHA-1, EHA-2, EHA-3 and EHA-4 samples are presented in Fig. 6. TGA plots of all the prepared samples revealed gradual weight loss due to the liberation of surface adsorbed water and carbonate molecules. All the samples showed three steps of weight loss, first exothermic weight loss observed in between ~34 and 180 °C for all samples is ascribed to the dehydration of the prepared samples and evaporation of physically/surface adsorbed water molecules. The second weight loss observed between ~180 and 900 °C is due to the removal of chemisorbed water and gradual elimination of carbonate molecules. The final weight loss of all the samples observed in the temperature range of ~900–1200 °C corresponds to the decomposition of the HA phase into β – tricalcium phosphate (β-TCP) due to removal of the structural OH^- group. Table 3 shows the temperature and its corresponding weight loss percentage of the prepared samples. It is noted that EHA-1 showed high weight loss in first and second steps which clearly indicates it contains a large amount of water molecules and carbonate content.

3.6. BET

Fig. 7 shows the plots of N_2 adsorption-desorption isotherm, Brunauer–Emmett–Teller (BET) surface area (inset in Fig. 7(a)) and pore size distribution of the prepared samples. Herein, the BET surface area plot of all the samples showed a linear variation which pointed out the accuracy in the quantitative measurement of surface area. The BET surface area of the EHA, EHA-1, EHA-2, EHA-3 and EHA-4 samples was observed as 54.74, 5.97, 33.57, 87.96 and 30.38 m^2/g, respectively. In general, the surface area of a material mainly depends upon the particle shape and size [40]. The obtained results clearly state that HA prepared in the presence of organic modifiers can change the surface area by controlling the shape and size of HA nanoparticles. Herein, Fig. 7(a) shows adsorption isotherm of all the samples which revealed type IV

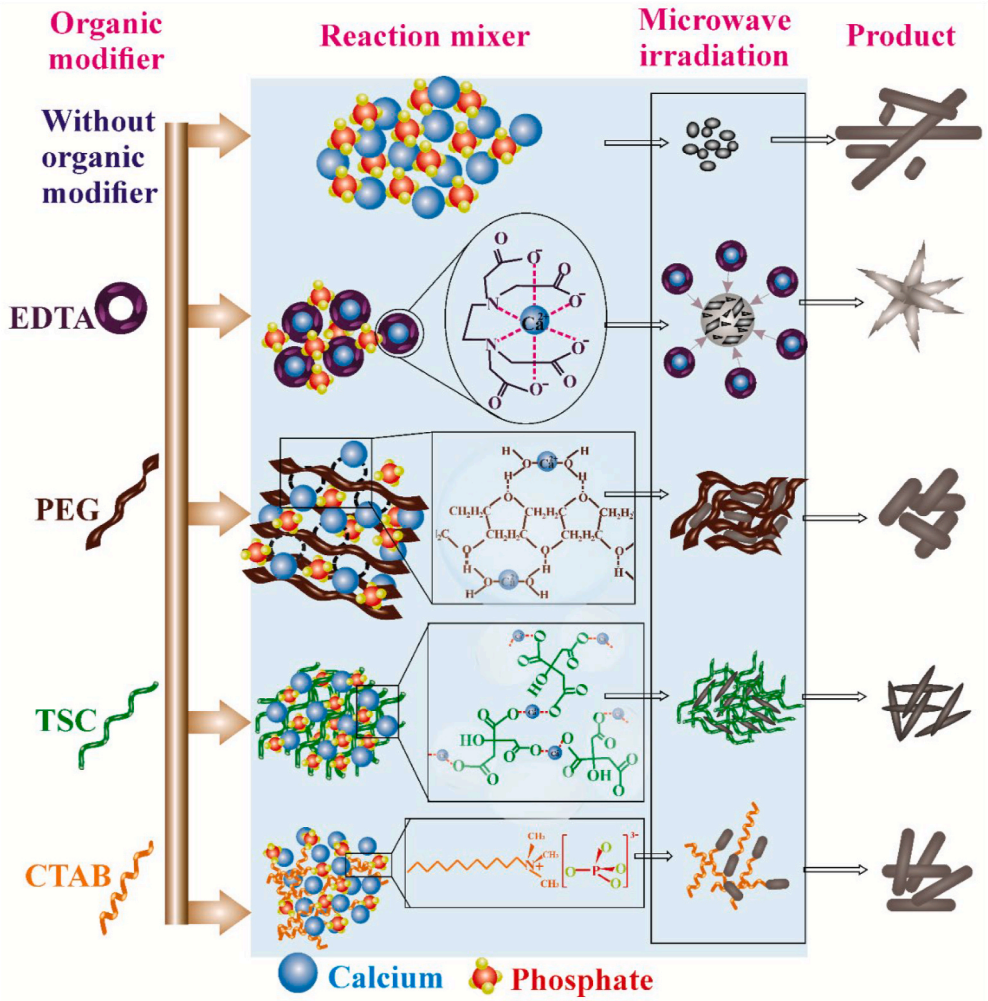

Fig. 10. Schematic representation of the formation of HA under microwave irradiation (2.2 kW) in the presence of different organic modifiers

physisorption isotherm according to the IUPAC classification [41]. This result clearly represents that the prepared samples are mesoporous materials. Fig. 7(b) shows the pore volume and pore diameter of the prepared samples. The Barrett-Joyner-Halenda (BJH) method was used to calculate the pore volume of samples. The pore volume of EHA, EHA-1, EHA-2, EHA-3 and EHA-4 were found to be 0.47, 0.03, 0.35, 0.58 and 0.24 respectively. Average pore diameter was found to be 221.04, 079.87, 262.69, 279.83 and 181.36 Å for EHA, EHA-1, EHA-2, EHA-3 and EHA-4 samples, respectively. According to IUPAC classification, the observed hysteresis loop clearly shows that the EHA contains cylindrical pore channels whereas other samples have slit shaped pore channels [41,42].

3.7. Cytocompatibility

Fig. 8 displays the cell viability of fibroblast NIH 3T3 cells cultured with different dosages of prepared samples. It is obvious that the prepared samples exhibited good cell viability for the different dosages of the samples. All the examined samples exhibited cell viability of above 82%. Cell viability of the samples (EHA to EHA-3) decreased with increasing concentration of the samples but EHA-4 sample maintained cell viability above 98% for all concentrations. However, slight variation in the cell viability is observed between the samples which may be attributed to their internal characteristics.

3.8. Cell adhesion

Cell attachment on the disc surface of EHA is a vital prerequisite stage for the growth of cells, migration and other functions. Fig. 9 shows the FESEM micrographs of the cells cultured on prepared disc samples for 24 h. All the samples exhibit suitable cell attachment on the disc surface. However, the EHA-4 sample showed less cell attachment than the other four samples. The presence of trace ions (Mg, Si, Na and CO_3^{2-}) inherited from the eggshell is believed to significantly enhance the biomineralization, cell proliferation and osteogenic properties of HA [43,44].

In recent years, material scientists are interested in the microwave method of material synthesis since it is an efficient and quick way to synthesize inorganic nanoparticles. Recently, our research group has designed and fabricated a microwave reactor capable of operating at 2.2 kW. In the present study, we have conducted the synthesis of mesoporous HA nanoparticles with different sizes and shape using some organic modifiers (Fig. 10) employing the above mentioned custom built microwave reactor in 5 min.

During synthesis size and shape of the HA, particles can be controlled using organic modifiers. The organic modifiers such as EDTA, PEG and TSC interact with calcium ions to make complex forms. The polyamino carboxylic acid of EDTA (hexadentate unit) reacts with Ca^{2+} to form a Ca-EDTA complex [45], PEG is a weak chelating and non-ionic organic modifier and chelate the Ca^{2+} ions in the form of PEG-O-Ca^{2+}-O-PEG [46], while citrate ion reacts with Ca^{2+} ions to form calcium citrate complex [36]. These complexes reduce the availability of free Ca^{2+} ions

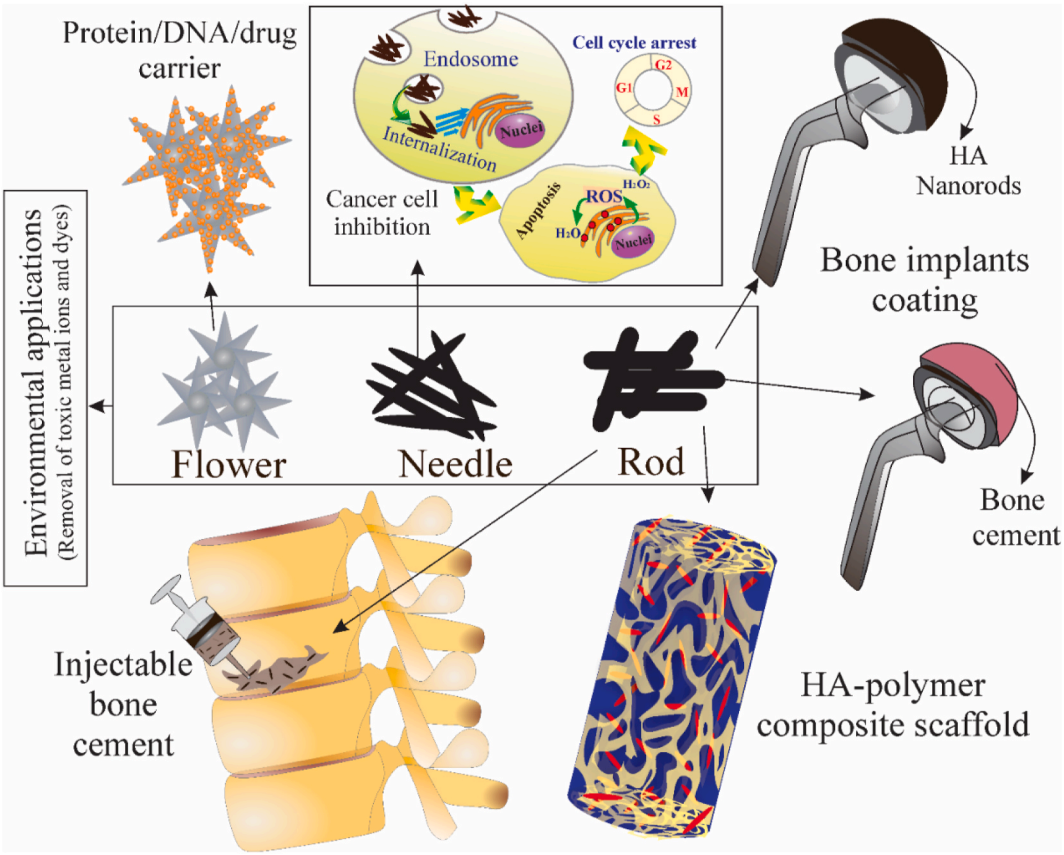

Fig. 11. Schematic diagram represents the different applications of various size and shape of HA nanoparticle

and inhibit the formation of HA at ambient temperature. The anionic organic modifier CTAB belongs to the soft template category; it, interacts with water to form positive charge micelles which react with the negatively charged PO_4^{3-} ions to form CTA^+-PO_4^{3-} due to strong electrostatic interaction [14,47]. Under microwave irradiation or thermal impact, the reaction mixture containing calcium complex releases Ca^{2+} ions which immediately react with phosphate and phosphate complex releases PO_4^{3-} ions which abruptly react with calcium to form HA crystal with controlled size and shape. The mechanism of formation of flower like HA in presence of EDTA was previously reported by several researchers [45,48,49]. Jung Sang Cho et al., reported the spherical, rod and fibre like HA nanoparticles formed in presence of different concentration of PEG organic modifiers [50]. Xiaoying Jin et al., studied the formation of HA nanorods with various aspect ratio through the hydrothermal method in the presence of sodium citrate organic modifier [36]. YingJun Wang et al., explained the formation mechanism of HA nanorods in the presence of CTAB surfactant [51].

HA nanoparticles with different sizes and shapes find wide application in hard tissue replacement, drug/protein/DNA carrier, etc. Xin-Yu Zhao and co-workers reported that flower like nanostructured HA has high adsorption capacity of proteins like bovine serum albumin-165 mg/g, hemoglobin-164 mg/g and DNA (fish sperm DNA-112 mg/g) [52]. Further, it has exhibited pH dependent protein release behaviour, revealing that the flower like morphology is suitable for physio-pathological pH responsive drug carrier application. Rod like HA nanoparticles are reported to enhance the cell attachment and migration leading to osteogenic efficacy. For example, osteogenic bioactivity of the rod shaped HA nanoparticle studied by Yulin Li et al. showed that stem cells could efficiently adsorb on less crystalline nanorods that mimic the natural HA. Ca^{2+} and PO_4^{3-} ions released by the partial dissolution of the HA nanorods at an acidic lysosomal condition regulate the osteogenic activity of stem cells [53]. HA nanorods are reinforced as an inorganic material in the composite scaffold to make bone substitutes for bone regeneration. In fact, HA nanorod addition in a polymeric material can increase mechanical properties and stimulate new bone formation [12]. Zandi et al. studied the biological and mechanical properties of HA nanorod reinforced gelatin composite scaffold fabricated using the freeze drying method. The obtained HA-gelatin composite scaffold increased the cell attachment and migration as compared to a pure gelatin scaffold [54].

Yubei Qiu et al. prepared bone morphogenetic protein-2 (BMP-2) loaded mesoporous HA nanorods mixed with silk fibroin/chitosan suspension and it was used to fabricate composite scaffold by freeze drying method. The presence of mesoporous HA nanorods induced *in vitro* osteogenic differentiation and promoted *in vivo* osteogenic efficacy. Furthermore, the mesoporous HA composite scaffold revealed the sustained release of BMP-2 and the concentration of BMP-2 release contributed to the desired bioactivity and improved osteogenic efficacy [55]. Li et al. reported the PEG surfactant assisted synthesis of HA nanorods where they introduced HA nanorods into polyurethane based injectable bone cement which showed enhanced bioactivity and mechanical properties towards osteoporosis management [56]. Also, Che et al. prepared composite bone cement using poly methyl methacrylate and rod like HA nanoparticles, which revealed an improved degree of bone mineralization and proliferation of bone progenitor cells [57].

On the other hand, nano HA is widely used in environmental applications because it reveals excellent adsorption, surface reactive and ionic exchange properties. For example, removal of Pb(II) ions from waste water by the sphere and rod shaped HA nanoparticles reported by Bharath et al. clearly indicated that HA nanoparticle of rod shape adsorbed more Pb(II) ions from waste water as compared to spherical one [58]. Varaprasad and co-workers studied the acidic blue 113 dye removal from waste water using rod like HA based hydrogel nanocomposite [59]. Inhibition ability of breast cancer cell growth by HA

Table 4
Size and shape of HA particles synthesized in presence of various organic modifiers by different methods.

Starting materials		Method of synthesis and conditions			Particle shape & size		Ref.
Chemical formula	Organic modifier	Method	pH	Time	Shape	Size	
$Ca(NO_3)_2{\cdot}4H_2O$ Na_2HPO_4	EDTA	Microwave 700 W	13	30 min	leaf-like flake	L: 1–2 μm W:150–200 nm	[62]
$Ca(NO_3)_2{\cdot}4H_2O$ Na_2HPO_4	EDTA	Microwave 600 W	10	19 min	Rod	D: ~5 nm L: ~15 nm	[49]
					Elliptical	15–17 nm × 25–28 nm	
$Ca(NO_3)_2{\cdot}4H_2O$ Na_2HPO_4	EDTA	Microwave 750 W	between 9 and 14	30 min	Rod	D: ~200 nm	[63]
Eggshell Na_2HPO_4	EDTA	Microwave 600 W	13	10 min	Flower	L:0.5–1 μm W:100–200 nm	[48]
$Ca(NO_3)_2{\cdot}4H_2O$ $(NH_4)_2HPO_4$ NH_4F	TSC	Microwave 600 W	10	25 min	Rod	L:26 ± 3 nm W:9 ± 2 nm	[64]
Eggshell Na_2HPO_4 (Previous work)	EDTA	Microwave reactor 2.2 kW	13	5 min	Flower	2 μm–3 μm	[34]
$Ca(NO_3)_2{\cdot}4H_2O$ Na_2HPO_4	EDTA	Hydrothermal 120 °C	5 and 12	12 h	Needle and rod	~50–200 nm	[65]
$Ca(NO_3)_2$ $(NH_4)_2HPO_4$	PEG-400 PEG-6000 PEG-20000	Hydrothermal 150 °C	11	40 h	Rod (PEG-400)	L: ~30–130 nm D: ~15–35 nm	[66]
					Rod (PEG-6000)	L: ~30–120 nm D: ~20–30 nm	
					Rod (PEG-20000)	L: ~30–170 nm D: ~15–35 nm	
$Ca(NO_3)_2{\cdot}4H_2O$ $Na_3PO_4{\cdot}12H_2O$	TSC	Hydrothermal 150 °C	Not stated	24 h	Rod (Ct/Ca:1/3)	L: 49 nm D: 13 nm	[36]
					Rod (Ct/Ca:4/3)	L: 44 nm D: 9 nm	
$Ca(NO_3)_2$ Na_3PO_4	CTAB	Hydrothermal 150 °C	Not stated	10 h	Rod	L: 150 nm	[46]
$CaCl_2{\cdot}2H_2O$ $(NH_4)_2HPO_4$	CTAB and PEG-6000	Hydrothermal 180 °C	10.5	24 h	Rod (CTAB) Chain (PEG-6000)	L: 250 nm D: 30 nm L: 180 nm D: 20 nm	[58]
$CaCl_2{\cdot}2H_2O$ $(NH_4)_2HPO_4$	CTAB	Hydrothermal 180 °C	12	12 h	Rod	5–50 nm	[67]
$CaCl_2$ H_3PO_4	CTAB	Hydrothermal 150 °C	9	12 h	Rod	L: 1125 nm D: 60 nm	[51]
$Ca(NO_3)_2{\cdot}4H_2O$ $(NH_4)_2HPO_4$	CTAB	Hydrothermal 150 °C	8	12 h	Nanowire	L: 600 nm D: 33 nm	[68]
Eggshell HCl Na_2HPO_4	CTAB	Hydrothermal 180 °C	Between 9 and 12	12 h	Rod	L: 161 ± 44 nm D: 52 ± 8 nm	[43]
$Na_2HPO_4{\cdot}2H_2O$ $CaCl_2$	CTAB	Hydrothermal 180 °C	Between 9.5 and 11	18 h	Rod	L: 136 nm D: 29 nm	[69]
Eggshell H_3PO_4	CTAB	Hydrothermal 160 °C	12	10 h	Rod	100–300 nm	[37]
$Ca(NO_3)_2{\cdot}4H_2O$ $(NH_4)_2HPO_4$	CTAB/PEG 600	Hydrothermal 120 °C	11	22 h	Rod (CTAB) Dandelion (CTAB &PEG 600)	D: 50–120 nm D: 80–150 nm	[70]
$Ca(NO_3)_2{\cdot}4H_2O$ $(NH_4)_2HPO_4$	EDTA/monoethanolamine	Hydrothermal 200 °C	10	7 h	Bundles of rod	L: ~10 μm W: ~1 μm	[71]
$Ca(NO_3)_2{\cdot}4H_2O$ $(NH_4)_2HPO_4$	Trisodiun citrate dihydrate (Ct)/CTAB	Hydrothermal 180 °C	5	24 h	Micro flake [Ct/CTAB (1/1)]	~ 2 μm	[72]
$Ca(NO_3)_2{\cdot}4H_2O$ $(NH_4)_2HPO_4$	CTAB	Microwave hydrothermal 200 °C	10	30 min,	Rod	L: 136.52 nm D: 43.17 nm	[73]
$Ca(NO_3)_2{\cdot}4H_2O$ Na_2HPO_4	CTAB/Sodium salicylate	Reflux 100 °C	11.5	2 h	Rod	L:100–500 nm D: ~ 50 nm	[74]
$CaCl_2$ $K_2HPO_4{\cdot}3H_2O$	CTAB	Reflux 120 °C	12	24 h	Rod	L: 22 nm D: 68.9 nm	[14]
$CaCl_2{\cdot}2H_2O$ K_2HPO_4	EDTA	Reflux 140 °C	9	120 h	Elongated crystal	D: 0.1 m L: 1.5 μm	[75]
$CaCl_2{\cdot}2H_2O$ K_2HPO_4	CTAB	Reflux 83 ± 2 °C	12	24 h	Rod	L: 500 nm-2 μm D:20–50 nm	[76]
$CaCl_2$ $K_2HPO_4{\cdot}3H_2O$	CTAB	Reflux 120 °C	12	24 h	Rod	L: 500–1000 nm T: 50–100 nm	[77]
$CaCl_2{\cdot}2H_2O$ Na_2HPO_4	TSC	Precipitation 80 °C	8.5	96 h	Platy crystal	L:38.9 ± 8.0 nm W:28.7 ± 4.2 nm T: 6.1 ± 2.2 nm	[78]
$Ca(NO_3)_2{\cdot}4H_2O$ $(NH_4)_2HPO_4$ NH_4F, Fe_3O_4	TSC	Precipitation Room temperature	10	24 h	Rod	30 nm	[79]
$Ca(NO_3)_2{\cdot}4H_2O$ $(NH_4)_2HPO_4$	CTAB	Precipitation 80 °C	12	24 h	Rod	L: 75–150 nm D: 10–25 nm	[80]

(continued on next page)

Table 4 (*continued*)

Starting materials		Method of synthesis and conditions			Particle shape & size		Ref.
Chemical formula	Organic modifier	Method	pH	Time	Shape	Size	
$Ca(NO_3)_2$ $(NH_4)_3PO_4$	TSC	Precipitation 90 °C	Between 7 and 8.5	54 min	Needle	L: 100–150 nm D: 10–20 nm	[81]
$CaCl_2$ Na_2HPO_4	CTAB	Wet precipitation 20 °C	9.5 ± 0.5	24 h	Spherical	D: 80 ± 12 nm	[82]
$Ca(H_2PO_4)_2{\cdot}H_2O$ $Ca(OH)_2$	PEG-20000	One step calcination 900 °C	Not stated	30 min	Not stated	50–80 nm	[83]
Eggshell derived CaO HNO_3 Na_2HPO_4	EDTA (✳) PEG (#) TSC (@) CTAB (֍)	Microwave reactor 2.2 kW	<10	5 min	Rod (Without organic modifier) Flower (✳) Rod (#) Needle (@) Rod (֍)	L: 40 - 600 nm W: 34 ± 10 nm 1.67 ± 0.12 μm L: 31 ± 8 nm W:8 ± 1 nm L:32 ± 8 nm W:3 ± 1 nm L:68 ± 20 nm W:10 ± 3 nm	Present work

L: Length, D: Diameter, W: Width, T: Thickness

nanoparticles of three different morphologies under *in vitro* conditions revealed that needle HA nanoparticles reduced the growth and proliferation of breast cancer cell lines by more than 73% [60]. Moreover, needle like HA nanoparticles has high surface charge, roughness and adhesion strength which significantly enable the growth of osteoblast (*in vitro*) and *in vivo* osteointegration efficacy of scaffold in rabbit model [61]. Thus, research community is showing more focus on obtaining HA nanoparticles with various size and shape to prepare bone substitutes with suitable properties for biomedical applications. The schematic shown in Fig. 11 clearly reveal the significant role of size and shape of HA nanoparticles for various applications.

The size and shape of HA particles synthesized in the presence of the organic modifiers employed in the present study by different methods reported in the literature is listed in Table 4. As observed from the table, the time consumed for the synthesis is from few hours to several hours when the method adopted was hydrothermal, reflux, precipitation, *etc*. The microwave reactor we utilized consumed just 5 min for the synthesis process. Therefore, eggshell derived HA nanoparticles with suitable characteristics for various biomedical applications can be rapidly synthesized by choosing appropriate organic modifier and our custom built microwave reactor.

4. Conclusion

In summary, we have synthesized mesoporous carbonated HA using eggshell biowaste as the calcium source *via* a custom built pilot scale microwave reactor in 5 min in the presence and absence of organic modifiers, employing the optimized parameters from our previous work. HA synthesized without organic modifier resulted in inhomogeneous sized rods of HA. While the presence of organic modifier controlled the physicochemical properties like particle size, surface area, morphology, mesoporous nature, *etc*. Micron sized flower like HA formed with EDTA as the modifier. However, the other organic modifiers produced rods or needles of typical size less than 100 nm. The *in vitro* cytotoxicity experiments of the prepared HA samples on fibroblast NIH 3T3 cell line clearly evidenced their excellent biocompatibility and revealed good cell attachment. Thus the custom built pilot scale microwave reactor is capable of producing eggshell derived HA rapidly with favourable characteristics in the presence of a suitable organic modifier for developing bone fillers, drug/protein delivery carriers, and tissue engineering scaffolds.

Declaration of competing interest

None.

Acknowledgement

The authors (E.K. Girija, D. Muthu and V.S. Kattimani) express their sincere thanks to Department of Science and Technology (DST), New Delhi, India (Project Ref. Nos. DST/TSG/WM/2015/576/G and DST/TDT/WMT/AgWaste/2021/01(G)) for financial support. The authors thank DST-FIST, India for providing XRD facility.

References

[1] S. Ha, H.L. Jang, K.T. Nam, G.R. Beck, Nano-hydroxyapatite modulates osteoblast lineage commitment by stimulation of DNA methylation and regulation of gene expression, Biomaterials 65 (2015) 32–42, https://doi.org/10.1016/j.biomaterials.2015.06.039.

[2] H. Nosrati, R.S. Mamoory, D.Q.S. Le, C.E. Bünger, R.Z. Emameh, F. Dabir, Gas injection approach for synthesis of hydroxyapatite nanorods via hydrothermal method, Mater. Char. 159 (2020), 110071, https://doi.org/10.1016/j.matchar.2019.110071.

[3] P. Terzioğlu, H. Öğüt, A. Kalemtaş, Natural calcium phosphates from fish bones and their potential biomedical applications, Mater. Sci. Eng. C 91 (2018) 899–911, https://doi.org/10.1016/j.msec.2018.06.010.

[4] F. Castro, A. Ferreira, F. Rocha, A. Vicente, J.A. Teixeira, Continuous-Flow precipitation of hydroxyapatite at 37 °C in a meso oscillatory flow reactor, Ind. Eng. Chem. Res. 52 (2013) 9816–9821, https://doi.org/10.1021/ie400710b.

[5] G. Montalbano, G. Molino, S. Fiorilli, C. Vitale-Brovarone, Synthesis and incorporation of rod-like nano-hydroxyapatite into type I collagen matrix: A hybrid formulation for 3D printing of bone scaffolds, J. Eur. Ceram. Soc. 40 (2020) 3689–3697, https://doi.org/10.1016/j.jeurceramsoc.2020.02.018.

[6] N. Horiuchi, K. Shibata, H. Saito, Y. Iwabuchi, N. Wada, K. Nozaki, K. Hashimoto, Y. Tanaka, A. Nagai, K. Yamashita, Size control synthesis of hydroxyapatite plates and their application in the preparation of highly oriented films, Cryst. Growth Des. 18 (2018) 5038–5044, https://doi.org/10.1021/acs.cgd.8b00480.

[7] D. Liao, W. Zheng, X. Li, Q. Yang, X. Yue, L. Guo, G. Zeng, Removal of lead(II) from aqueous solutions using carbonate hydroxyapatite extracted from eggshell waste, J. Hazard Mater. 177 (2010) 126–130, https://doi.org/10.1016/j.jhazmat.2009.12.005.

[8] A. Das, D. Pamu, A comprehensive review on electrical properties of hydroxyapatite based ceramic composites, Mater. Sci. Eng. C 101 (2019) 539–563, https://doi.org/10.1016/j.msec.2019.03.077.

[9] H. Cao, L. Zhang, H. Zheng, Z. Wang, Hydroxyapatite nanocrystals for biomedical applications, J. Phys. Chem. C 114 (2010) 18352–18357, https://doi.org/10.1021/jp106078b.

[10] Q. Wang, J. Yan, J. Yang, B. Li, Nanomaterials promise better bone repair, Mater. Today 19 (2016) 451–463, https://doi.org/10.1016/j.mattod.2015.12.003.

[11] G.S. Kumar, G. Karunakaran, E.K. Girija, E. Kolesnikov, N. Van Minh, M. V. Gorshenkov, D. Kuznetsov, Size and morphology-controlled synthesis of mesoporous hydroxyapatite nanocrystals by microwave-assisted hydrothermal method, Ceram. Int. 44 (2018) 11257–11264, https://doi.org/10.1016/j.ceramint.2018.03.170.

[12] G. Molino, M.C. Palmieri, G. Montalbano, S. Fiorilli, C. Vitale-Brovarone, Biomimetic and mesoporous nano-hydroxyapatite for bone tissue application: a short review, Biomed. Mater. 15 (2020) 22001, https://doi.org/10.1088/1748-605X/ab5f1a.

[13] S. Ucar, S.H. Bjørnøy, D.C. Bassett, B.L. Strand, P. Sikorski, J.-P. Andreassen, Formation of hydroxyapatite via transformation of amorphous calcium phosphate in the presence of alginate additives, Cryst. Growth Des. 19 (2019) 7077–7087, https://doi.org/10.1021/acs.cgd.9b00887.

[14] K. Shiba, S. Motozuka, T. Yamaguchi, N. Ogawa, Y. Otsuka, K. Ohnuma, T. Kataoka, M. Tagaya, Effect of cationic surfactant micelles on hydroxyapatite nanocrystal Formation: an investigation into the inorganic–organic interfacial interactions, Cryst. Growth Des. 16 (2016) 1463–1471, https://doi.org/10.1021/acs.cgd.5b01599.
[15] M. Sadat-Shojai, M.-T. Khorasani, E. Dinpanah-Khoshdargi, A. Jamshidi, Synthesis methods for nanosized hydroxyapatite with diverse structures, Acta Biomater. 9 (2013) 7591–7621, https://doi.org/10.1016/j.actbio.2013.04.012.
[16] A. Rajendran, R. Kulandaivelu, S.N.T.S. Nellaiappan, Crystalline selenite substituted carbonated hydroxyapatite nanorods: synthesis, characterization, evaluation of bioactivity and cytotoxicity, Int. J. Appl. Ceram. Technol. 14 (2017) 68–76, https://doi.org/10.1111/ijac.12619.
[17] G.C. Koumoulidis, A.P. Katsoulidis, A.K. Ladavos, P.J. Pomonis, C.C. Trapalis, A. T. Sdoukos, T.C. Vaimakis, Preparation of hydroxyapatite via microemulsion route, J. Colloid Interface Sci. 259 (2003) 254–260, https://doi.org/10.1016/S0021-9797(02)00233-3.
[18] M.L. Montero, A. Sáenz, J.G. Rodríguez, J. Arenas, V.M. Castaño, Electrochemical synthesis of nanosized hydroxyapatite, J. Mater. Sci. 41 (2006) 2141–2144, https://doi.org/10.1007/s10853-006-5231-x.
[19] M.N. Hassan, M.M. Mahmoud, A.A. El-Fattah, S. Kandil, Microwave-assisted preparation of Nano-hydroxyapatite for bone substitutes, Ceram. Int. 42 (2016) 3725–3744, https://doi.org/10.1016/j.ceramint.2015.11.044.
[20] X. Guo, H. Yan, S. Zhao, Z. Li, Y. Li, X. Liang, Effect of calcining temperature on particle size of hydroxyapatite synthesized by solid-state reaction at room temperature, Adv. Powder Technol. 24 (2013) 1034–1038, https://doi.org/10.1016/j.apt.2013.03.002.
[21] R. Jayasree, K. Madhumathi, D. Rana, M. Ramalingam, R.P. Nankar, M. Doble, T.S. S. Kumar, Development of egg shell derived carbonated apatite nanocarrier system for drug delivery, J. Nanosci. Nanotechnol. 18 (2018) 2318–2324, https://doi.org/10.1166/jnn.2018.14377.
[22] M.B. Kannan, K. Ronan, Conversion of biowastes to biomaterial: an innovative waste management approach, Waste Manag. 67 (2017) 67–72, https://doi.org/10.1016/j.wasman.2017.05.045.
[23] V.H. Ingole, K. Hany Hussein, A.A. Kashale, K. Ghule, T. Vuherer, V. Kokol, J.-Y. Chang, Y.-C. Ling, A. Vinchurkar, H.N. Dhakal, A.V. Ghule, Ultrasound-assisted green economic synthesis of hydroxyapatite nanoparticles using eggshell biowaste and study of mechanical and biological properties for orthopedic applications, J. Biomed. Mater. Res. 105 (2017) 2935–2947, https://doi.org/10.1002/jbm.a.36146.
[24] K. Huang, J. Hou, Z. Gu, J. Wu, Egg-White-/Eggshell-Based biomimetic hybrid hydrogels for bone regeneration, ACS Biomater. Sci. Eng. 5 (2019) 5384–5391, https://doi.org/10.1021/acsbiomaterials.9b00990.
[25] R. Jayasree, T.S. Sampath Kumar, K. Pavani Siva Kavya, P. Rakesh Nankar, D. Mukesh, Self setting bone cement formulations based on egg shell derived tetracalcium phosphate bioceramics, Bioceram. Dev. Appl. 5 (2015), 1000084, https://doi.org/10.4172/2090-5025.1000084.
[26] P. Dadhich, B. Das, P. Pal, P.K. Srivas, J. Dutta, S. Ray, S. Dhara, A simple approach for an eggshell-based 3D-printed osteoinductive multiphasic calcium phosphate scaffold, ACS Appl. Mater. Interfaces 8 (2016) 11910–11924, https://doi.org/10.1021/acsami.5b11981.
[27] V.A. Apalangya, V.K. Rangari, B.J. Tiimob, S. Jeelani, T. Samuel, Eggshell based nano-engineered hydroxyapatite and poly(lactic) acid electrospun fibers as potential tissue scaffold, International Journal of Biomaterials. 2019 (2019) 1–11, https://doi.org/10.1155/2019/6762575.
[28] S.K. Padmanabhan, L. Salvatore, F. Gervaso, M. Catalano, A. Taurino, A. Sannino, A. Licciulli, Synthesis and characterization of collagen scaffolds reinforced by eggshell derived hydroxyapatite for tissue engineering, J. Nanosci. Nanotechnol. 15 (2015) 504–509, https://doi.org/10.1166/jnn.2015.9489.
[29] Y.E. Arslan, T. Sezgin Arslan, B. Derkus, E. Emregul, K.C. Emregul, Fabrication of human hair keratin/jellyfish collagen/eggshell-derived hydroxyapatite osteoinductive biocomposite scaffolds for bone tissue engineering: From waste to regenerative medicine products, Colloids Surf. B Biointerfaces 154 (2017) 160–170, https://doi.org/10.1016/j.colsurfb.2017.03.034.
[30] A.H. Verma, T.S.S. Kumar, K. Madhumathi, Y. Rubaiya, M. Ramalingan, M. Doble, Curcumin releasing eggshell derived carbonated apatite nanocarriers for combined Anti-cancer, Anti-inflammatory and bone regenerative therapy, J. Nanosci. Nanotechnol. 19 (2019) 6872–6880, https://doi.org/10.1166/jnn.2019.16640.
[31] G.S. Kumar, E.K. Girija, Flower-like hydroxyapatite nanostructure obtained from eggshell: a candidate for biomedical applications, Ceram. Int. 39 (2013) 8293–8299, https://doi.org/10.1016/j.ceramint.2013.03.099.
[32] R. Vani, S.B. Raja, T.S. Sridevi, K. Savithri, S.N. Devaraj, E.K. Girija, A. Thamizhavel, S.N. Kalkura, Surfactant free rapid synthesis of hydroxyapatite nanorods by a microwave irradiation method for the treatment of bone infection, Nanotechnology 22 (2011), 285701, https://doi.org/10.1088/0957-4484/22/28/285701.
[33] T. Liang, J. Qian, Y. Yuan, C. Liu, Synthesis of mesoporous hydroxyapatite nanoparticles using a template-free sonochemistry-assisted microwave method, J. Mater. Sci. 48 (2013) 5334–5341, https://doi.org/10.1007/s10853-013-7328-3.
[34] D. Muthu, G.S. Kumar, V.S. Kattimani, V. Viswabaskaran, E.K. Girija, Optimization of a lab scale and pilot scale conversion of eggshell biowaste into hydroxyapatite using microwave reactor, Ceram. Int. 46 (2020) 25024–25034, https://doi.org/10.1016/j.ceramint.2020.06.288.
[35] C. Qiu, X. Xiao, R. Liu, Biomimetic synthesis of spherical nano-hydroxyapatite in the presence of polyethylene glycol, Ceram. Int. 34 (2008) 1747–1751, https://doi.org/10.1016/j.ceramint.2007.06.001.
[36] X. Jin, J. Zhuang, Z. Zhang, H. Guo, J. Tan, Hydrothermal synthesis of hydroxyapatite nanorods in the presence of sodium citrate and its aqueous colloidal stability evaluation in neutral pH, J. Colloid Interface Sci. 443 (2015) 125–130, https://doi.org/10.1016/j.jcis.2014.12.010.
[37] K. Prabakaran, S. Rajeswari, Spectroscopic investigations on the synthesis of nano-hydroxyapatite from calcined eggshell by hydrothermal method using cationic surfactant as template, Spectrochim. Acta Mol. Biomol. Spectrosc. 74 (2009) 1127–1134, https://doi.org/10.1016/j.saa.2009.09.021.
[38] G.S. Kumar, A. Thamizhavel, Y. Yokogawa, S.N. Kalkura, E.K. Girija, Synthesis, characterization and in vitro studies of zinc and carbonate co-substituted nano-hydroxyapatite for biomedical applications, Mater. Chem. Phys. 134 (2012) 1127–1135, https://doi.org/10.1016/j.matchemphys.2012.04.005.
[39] R. Sun, L. Yang, Y. Zhang, F. Chu, G. Wang, Y. Lv, K. Chen, Novel synthesis of AB-type carbonated hydroxyapatite hierarchical microstructures with sustained drug delivery properties, CrystEngComm 18 (2016) 8030–8037, https://doi.org/10.1039/C6CE01494A.
[40] A. Anwar, I.U. Rehman, J.A. Darr, Low-temperature synthesis and surface modification of high surface area calcium hydroxyapatite nanorods incorporating organofunctionalized surfaces, J. Phys. Chem. C 120 (2016) 29069–29076, https://doi.org/10.1021/acs.jpcc.6b05878.
[41] K.S.W. Sing, Reporting physisorption data for gas/solid systems with special reference to the determination of surface area and porosity (Provisional), Pure Appl. Chem. 54 (1982) 2201–2218, https://doi.org/10.1351/pac198254112201.
[42] K.S.W. Sing, R.T. Williams, Physisorption hysteresis loops and the characterization of nanoporous materials, Adsorpt. Sci. Technol. 22 (2004) 773–782, https://doi.org/10.1260/0263617053499032.
[43] N.K. Nga, N.T. Thuy Chau, P.H. Viet, Facile synthesis of hydroxyapatite nanoparticles mimicking biological apatite from eggshells for bone-tissue engineering, Colloids Surf. B Biointerfaces 172 (2018) 769–778, https://doi.org/10.1016/j.colsurfb.2018.09.039.
[44] S. Bose, G. Fielding, S. Tarafder, A. Bandyopadhyay, Understanding of dopant-induced osteogenesis and angiogenesis in calcium phosphate ceramics, Trends Biotechnol. 31 (2013) 594–605, https://doi.org/10.1016/j.tibtech.2013.06.005.
[45] J. Liu, K. Li, H. Wang, M. Zhu, H. Xu, H. Yan, Self-assembly of hydroxyapatite nanostructures by microwave irradiation, Nanotechnology 16 (2005) 82–87, https://doi.org/10.1088/0957-4484/16/1/017.
[46] M. Salarian, M. Solati-Hashjin, S.S. Shafiei, A. Goudarzi, R. Salarian, A. Nemati, Surfactant-assisted synthesis and characterization of hydroxyapatite nanorods under hydrothermal conditions, Materials Science- Poland 27 (2009) 961–971.
[47] Y. Li, W. Tjandra, K.C. Tam, Synthesis and characterization of nanoporous hydroxyapatite using cationic surfactants as templates, Mater. Res. Bull. 43 (2008) 2318–2326, https://doi.org/10.1016/j.materresbull.2007.08.008.
[48] G.S. Kumar, A. Thamizhavel, E.K. Girija, Microwave conversion of eggshells into flower-like hydroxyapatite nanostructure for biomedical applications, Mater. Lett. 76 (2012) 198–200, https://doi.org/10.1016/j.matlet.2012.02.106.
[49] S.J. Kalita, S. Verma, Nanocrystalline hydroxyapatite bioceramic using microwave radiation: synthesis and characterization, Mater. Sci. Eng. C 30 (2010) 295–303, https://doi.org/10.1016/j.msec.2009.11.007.
[50] J.S. Cho, Y.C. Kang, Nano-sized hydroxyapatite powders prepared by flame spray pyrolysis, J. Alloys Compd. 464 (2008) 282–287, https://doi.org/10.1016/j.jallcom.2007.09.092.
[51] Y. Wang, J. Chen, K. Wei, S. Zhang, X. Wang, Surfactant-assisted synthesis of hydroxyapatite particles, Mater. Lett. 60 (2006) 3227–3231, https://doi.org/10.1016/j.matlet.2006.02.077.
[52] X.-Y. Zhao, Y.-J. Zhu, F. Chen, B.-Q. Lu, J. Wu, Nanosheet-assembled hierarchical nanostructures of hydroxyapatite: surfactant-free microwave-hydrothermal rapid synthesis, protein/DNA adsorption and pH-controlled release, CrystEngComm 15 (2013) 206–212, https://doi.org/10.1039/C2CE26315G.
[53] Y. Li, Y. Wang, Y. Li, W. Luo, J. Jiang, J. Zhao, C. Liu, Controllable synthesis of biomimetic hydroxyapatite nanorods with high osteogenic bioactivity, ACS Biomater. Sci. Eng. 6 (2020) 320–328, https://doi.org/10.1021/acsbiomaterials.9b00914.
[54] M. Zandi, H. Mirzadeh, C. Mayer, H. Urch, M.B. Eslaminejad, F. Bagheri, H. Mivehchi, Biocompatibility evaluation of nano-rod hydroxyapatite/gelatin coated with nano-HAp as a novel scaffold using mesenchymal stem cells, J. Biomed. Mater. Res. (2009) 9999A, https://doi.org/10.1002/jbm.a.32452. NA-NA.
[55] Y. Qiu, X. Xu, W. Guo, Y. Zhao, J. Su, J. Chen, Mesoporous hydroxyapatite nanoparticles mediate the release and bioactivity of BMP-2 for enhanced bone regeneration, ACS Biomater. Sci. Eng. 6 (2020) 2323–2335, https://doi.org/10.1021/acsbiomaterials.9b01954.
[56] K. Li, Y. Zuo, Q. Zou, L. Lin, L. Wang, B. Yang, F. Hu, J. Li, Y. Li, J. Li, Synthesis and characterization of injectable nano-hydroxyapatite/polyurethane composite cement effective formulations for management of osteoporosis, J. Nanosci. Nanotechnol. 16 (2016) 12407–12417, https://doi.org/10.1166/jnn.2016.13763.
[57] Y. Che, S. Min, M. Wang, M. Rao, C. Quan, Biological activity of hydroxyapatite/poly(methylmethacrylate) bone cement with different surface morphologies and modifications for induced osteogenesis, J. Appl. Polym. Sci. 136 (2019) 48188, https://doi.org/10.1002/app.48188.
[58] G. Bharath, A. Jagadeesh Kumar, K. Karthick, D. Mangalaraj, C. Viswanathan, N. Ponpandian, Shape evolution and size controlled synthesis of mesoporous hydroxyapatite nanostructures and their morphology dependent Pb(<scp>ii</scp>) removal from waste water, RSC Adv. 4 (2014) 37446–37457, https://doi.org/10.1039/C4RA06929C.

[59] K. Varaprasad, D. Nunez, M.M. Yallapu, T. Jayaramudu, E. Elgueta, P. Oyarzun, Nano-hydroxyapatite polymeric hydrogels for dye removal, RSC Adv. 8 (2018) 18118–18127, https://doi.org/10.1039/C8RA01887A.
[60] A. Seyfoori, S.M. Naghib, F. Molaabasi, Inhibitory effect comparison of the needle, spherical, and mesoporous hydroxyapatite nanoparticles on MCF-7 breast cancer cell line proliferation: an in vitro assay, Advances in Nanochemistry 2 (2020) 11–14, https://doi.org/10.22126/ANC.2020.4865.1020.
[61] V. Guarino, F. Veronesi, M. Marrese, G. Giavaresi, A. Ronca, M. Sandri, A. Tampieri, M. Fini, L. Ambrosio, Needle-like ion-doped hydroxyapatite crystals influence osteogenic properties of PCL composite scaffolds, Biomed. Mater. 11 (2016) 15018, https://doi.org/10.1088/1748-6041/11/1/015018.
[62] J. Liu, K. Li, H. Wang, M. Zhu, H. Yan, Rapid formation of hydroxyapatite nanostructures by microwave irradiation, Chem. Phys. Lett. 396 (2004) 429–432, https://doi.org/10.1016/j.cplett.2004.08.094.
[63] V.K. Mishra, S.K. Srivastava, B.P. Asthana, D. Kumar, Structural and spectroscopic studies of hydroxyapatite nanorods formed via microwave-assisted synthesis route, J. Am. Ceram. Soc. 95 (2012) 2709–2715, https://doi.org/10.1111/j.1551-2916.2012.05134.x.
[64] S. Karthi, G.S. Kumar, G.A. Kumar, D.K. Sardar, C. Santhosh, E.K. Girija, Microwave assisted synthesis and characterizations of near infrared emitting Yb/Er doped fluorapatite nanoparticles, J. Alloys Compd. 689 (2016) 525–532, https://doi.org/10.1016/j.jallcom.2016.08.005.
[65] R. Xin, F. Ren, Y. Leng, Synthesis and characterization of nano-crystalline calcium phosphates with EDTA-assisted hydrothermal method, Mater. Des. 31 (2010) 1691–1694, https://doi.org/10.1016/j.matdes.2009.01.048.
[66] H. Zhang, M. Liu, H. Fan, X. Zhang, Carbonated nano hydroxyapatite crystal growth modulated by poly(ethylene glycol) with different molecular weights, Cryst. Growth Des. 12 (2012) 2204–2212, https://doi.org/10.1021/cg200917y.
[67] M. Kermanian, M. Naghibi, S. Sadighian, One-pot hydrothermal synthesis of a magnetic hydroxyapatite nanocomposite for MR imaging and pH-Sensitive drug delivery applications, Heliyon 6 (2020), e04928, https://doi.org/10.1016/j.heliyon.2020.e04928.
[68] A.J. Nathanael, S.I. Hong, T.H. Oh, Y.H. Seo, D. Singh, S.S. Han, Enhanced cell viability of hydroxyapatite nanowires by surfactant mediated synthesis and its growth mechanism, RSC Adv. 6 (2016) 25070–25081, https://doi.org/10.1039/C6RA01155A.
[69] N.K. Nguyen, M. Leoni, D. Maniglio, C. Migliaresi, Hydroxyapatite nanorods: soft-template synthesis, characterization and preliminary in vitro tests, J. Biomater. Appl. 28 (2013) 49–61, https://doi.org/10.1177/0885328212437065.
[70] M. Salarian, M. Solati-Hashjin, S.S. Shafiei, R. Salarian, Z.A. Nemati, Template-directed hydrothermal synthesis of dandelion-like hydroxyapatite in the presence of cetyltrimethylammonium bromide and polyethylene glycol, Ceram. Int. 35 (2009) 2563–2569, https://doi.org/10.1016/j.ceramint.2009.02.031.
[71] K. Suchanek, A. Bartkowiak, M. Perzanowski, M. Marszałek, From monetite plate to hydroxyapatite nanofibers by monoethanolamine assisted hydrothermal approach, Sci. Rep. 8 (2018) 15408, https://doi.org/10.1038/s41598-018-33936-4.
[72] H. Yang, Y. Wang, Morphology control of hydroxyapatite microcrystals: synergistic effects of citrate and CTAB, Mater. Sci. Eng. C 62 (2016) 160–165, https://doi.org/10.1016/j.msec.2016.01.052.
[73] D. Sánchez-Campos, D. Mendoza-Anaya, M.I. Reyes-Valderrama, S. Esteban-Gómez, V. Rodríguez-Lugo, Cationic surfactant at high pH in microwave HAp synthesis, Mater. Lett. 265 (2020), 127416, https://doi.org/10.1016/j.matlet.2020.127416.
[74] G. Verma, K.C. Barick, N. Manoj, A.K. Sahu, P.A. Hassan, Rod-like micelle templated synthesis of porous hydroxyapatite, Ceram. Int. 39 (2013) 8995–9002, https://doi.org/10.1016/j.ceramint.2013.04.100.
[75] H. Arce, M.L. Montero, A. Sáenz, V.M. Castaño, Effect of pH and temperature on the formation of hydroxyapatite at low temperatures by decomposition of a Ca–EDTA complex, Polyhedron 23 (2004) 1897–1901, https://doi.org/10.1016/j.poly.2004.04.021.
[76] J.M. Coelho, J.A. Moreira, A. Almeida, F.J. Monteiro, Synthesis and characterization of HAp nanorods from a cationic surfactant template method, J. Mater. Sci. Mater. Med. 21 (2010) 2543–2549, https://doi.org/10.1007/s10856-010-4122-5.
[77] J. Yao, W. Tjandra, Y.Z. Chen, K.C. Tam, J. Ma, B. Soh, Hydroxyapatite nanostructure material derived using cationic surfactant as a template, J. Mater. Chem. 13 (2003) 3053, https://doi.org/10.1039/b308801d.
[78] J.M. Delgado-López, R. Frison, A. Cervellino, J. Gómez-Morales, A. Guagliardi, N. Masciocchi, Crystal size, morphology, and growth mechanism in bio-inspired apatite nanocrystals, Adv. Funct. Mater. 24 (2014) 1090–1099, https://doi.org/10.1002/adfm.201302075.
[79] S. Karthi, G.A. Kumar, D.K. Sardar, G.C. Dannangoda, K.S. Martirosyan, E.K. Girija, Fluorapatite coated iron oxide nanostructure for biomedical applications, Mater. Chem. Phys. 193 (2017) 356–363, https://doi.org/10.1016/j.matchemphys.2017.02.047.
[80] M. Khalid, M. Mujahid, S. Amin, R.S. Rawat, A. Nusair, G.R. Deen, Effect of surfactant and heat treatment on morphology, surface area and crystallinity in hydroxyapatite nanocrystals, Ceram. Int. 39 (2013) 39–50, https://doi.org/10.1016/j.ceramint.2012.05.090.
[81] C. Li, L. Zhao, J. Han, R. Wang, C. Xiong, X. Xie, Synthesis of citrate-stabilized hydrocolloids of hydroxyapatite through a novel two-stage method: A possible aggregates–breakdown mechanism of colloid formation, J. Colloid Interface Sci. 360 (2011) 341–349, https://doi.org/10.1016/j.jcis.2011.04.059.
[82] Y. Cai, Y. Liu, W. Yan, Q. Hu, J. Tao, M. Zhang, Z. Shi, R. Tang, Role of hydroxyapatite nanoparticle size in bone cell proliferation, J. Mater. Chem. 17 (2007) 3780, https://doi.org/10.1039/b705129h.
[83] Y. Tseng, C. Kuo, Y. Li, C. Huang, Polymer-assisted synthesis of hydroxyapatite nanoparticle, Mater. Sci. Eng. C 29 (2009) 819–822, https://doi.org/10.1016/j.msec.2008.07.028.